SAND2016-6323J

Phosphorous dimerization in GaP high-pressure polymorph

Barbara Lavina[1,2], Eunja Kim[2], Hyunchae Cynn[3], Philippe F. Weck[4], Kelly Seaborg[1,2], Emily Siska[1], Yue Meng[5], William Evans[3]

[1]*High Pressure Science and Engineering Center, University of Nevada, Las Vegas*
[2]*Department of Physics and Astronomy, University of Nevada, Las Vegas*
[3]*Lawrence Livermore National Laboratory*
[4]*Sandia National Laboratory*
[5] *HPCAT, Carnegie Institution of Washington*

We report on the experimental and theoretical characterization of a novel GaP polymorph formed by laser heating of a single crystal of GaP-II in its stable region near 43 GPa. Thereby formed unstrained multigrain sample at 43 GPa and 1300 K, allowed high-resolution crystallographic analysis. We find an oS24 as an energetically optimized crystal structure contrary to oS8 reported by Nelmes et al. (1997). Our DFT calculation confirms a stable existence of oS24 between 18 – 50 GPa. The emergence of the *oS*24 structure is related to the differentiation of phosphorous atoms between those forming P-P dimers and those forming P-Ga bonds only. Bonding anisotropy explains the symmetry lowering with respect to what is generally expected for semiconductors high-pressure polymorphs. The metallization of GaP does not occur through a uniform change of the nature of its bonds but through the formation of an anisotropic phase containing different bond types.

The high-pressure behavior of semiconductors has been extensively investigated since the 1960s after sharp decreases in resistivity revealed transitions to metallic states in all compounds [2,3]. Studies of the associated structural changes followed, with the aim of linking atomic arrangements to physical properties and uncover the systematic behavior of this important class of materials. Overall consensus on the polymorphism of group IV_A, III_A-V_A and II_B-VI_A semiconductors was reached in the early 2000s, structures and systematic trends are reviewed in several papers [4–9]. Major developments in the

field were not anticipated, nonetheless high resolution crystallographic analysis has been called for in order to achieve a better understanding of the true nature of the polymorphism [10], a task tackled in this work for GaP.

The III_A-V_A semiconductor crystallizes with the zinc blend structure (*cF*8) and undergoes a transition to a semimetallic state at ~22 GPa [3]. Powder diffraction methods were used to demonstrate that the phase transition associated with the metallization of GaP, as well as several other semiconductors, does not result in the β-Sn structure as previously thought [11] but instead in an orthorhombic structure with Pearson symbol *oS*8, which can be described as a distorted NaCl arrangement [12]. The site-disordered *oS*8 structure was proposed for GaP and GaAs, while its site-ordered counterpart was proposed for AlSb, InP, InAs, CdTe, HgTe, and HgSe. While diffraction data suggest that GaP-*oS*8 is long-range site-disordered [12,13], XAFS data show it is short-range ordered [13]. Recent calculations still consider the NaCl structure a possible GaP high-pressure polymorph [14,15], however earlier studies provide in-depth analysis of the instability of the phase [10,16] which has not been observed experimentally. Theoretical studies suggest a small stability range for the *cP*16 arrangement (simple cubic SC16) between the ambient pressure phase and the orthorhombic polymorph [16], the kinetic barrier associated with these first order phase transitions can explain the lack of experimental evidences of *cP*16.

The specimen used in this study was a thin light brown colored single crystal wafer. Trace metals analysis with ICPMS determined the sample contains 34.5μg/g of boron and no other detectable contaminants. Samples were compressed using diamond anvil cells and probed via x-ray diffraction. Between the anvils' culets, 300 μm in diameter, rhenium gaskets indented to ~40 μm thickness with 120 μm holes provided the sample chambers. In the powder diffraction experiment (pXRD) the sample was reduced to fine powder and was loaded under mineral oil. Pressure was determined using a copper equation-of-state (EOS) determined by comparing measured volume of Ne and Cu and slightly modified from Fei et al. EOS resulting a Vinet formulation for copper EOS, K_0=133.41 GPa, K_0'=5.3298, V_0=47.2299 A^3, Θ_0=319.2 K, γ_0=1.99, q=0.597 [17]. These parameters agree very well with a calculation by Greeff ([18]) and Wang et al. In the single crystal diffraction experiment (SXD) a fragment of the specimen along with gold fine powder and pre-pressurized neon gas [19] were loaded in the sample chamber. Pressure was gauged using gold's EOS [20]. The single crystal was heated at 43 GPa to promote re-crystallization using an online double-sided IR laser-heating setup in which temperature is determined from the emitted radiation [21]. The samples were probed using 33.168 keV (pXRD) and 33.169 keV (SXD) x-ray beams. Diffracted beams were

collected with MAR345-IP (pXRD) and MAR165-CCD (SXD) area detectors, which were calibrated using powder patterns of a CeO_2 standard. SXD data, with a resolution of 0.6 Å, were collected with the rotation method. Data reduction was performed with FIT2D [22], GSE_ADA and RSV [23]. Structural solution and refinements were carried out using Endeavour, and Shelxl [24].

First-principles total energy calculations were performed using the spin-polarized density functional theory (DFT) as implemented in the Vienna *ab initio* simulation package (VASP) [25]. The exchange-correlation energy was calculated using the generalized gradient approximation (GGA) with the parameterization of Perdew, Burke and Ernzerhof (PBE) [26]. The interaction between valence electrons and ionic cores was described by the projector augmented wave (PAW) method [27,28]. The Ga ($3d^{10}$, $4s^2$, $4p^1$) and P ($3s^2$, $3p^3$) electrons were treated explicitly as valence electrons in the Kohn-Sham (KS) equation and the remaining core electrons together with the nuclei were represented by PAW pseudopotentials. The plane-wave cutoff energy for the electronic wavefunctions was set to a value of 500 eV, ensuring the total energy of the system to be converged to within $1x10^{-5}$ eV/atom. A periodic unit cell containing 4, 8, 4, and 12 formula units was used in the calculations for *cF*8, *cP*16, *oS*8, and *oS*24, respectively. Electronic relaxation was performed with the conjugate gradient method accelerated using the Methfessel-Paxton Fermi-level smearing [29]. Ionic relaxation was carried out using the quasi-Newton method and the Hellmann-Feynman forces acting on atoms were calculated with a convergence tolerance set to 0.001 eV/Å. The Brillouin zone was sampled using the Monkhorst-Pack special k-point scheme [30] with a 7x7x7 mesh for structural optimization and total energy calculations.

Due to the different stress conditions generated by the different pressure transmitting media, the compression data of GaP-*cF*8 of the two experiments differ slightly (Fig. 1) The pressure of phase transition onset is slightly higher for the sample in hydrostatic conditions: at ~ 24.5 GPa, while the crystal does not show significant changes, the powder specimen shows new peaks while retaining peaks of the *cF*8 phase up to ~ 30 GPa. The bulk modulus of the *cF*8 phase was determined using the 14 data points from the SXD experiment applying the 3rd order Birch-Murnaghan EOS. We fixed the first derivative to the literature value 4.5 [16], the value theoretically determined by Mujica and Needs [9], obtaining a bulk modulus of 87.5 (6) GPa, in close agreement with our theoretical value of 83.5 GPa from DFT and Mujica and Needs' value (90 GPa) but rather different from other theoretical results (78.35 GPa with a K'_0 of 4.27 [14]). In agreement with previous results, pXRD data of the high-pressure phase were interpreted with the *oS*8 structure. GaP-*oS*8 compressibility was measured in fine steps (Fig. 1) up to ~ 50

GPa, the change in volume at 25 GPa is ~16 %. In the SXD experiment diffraction peaks of the high-pressure phase remained weak and very broad hindering the structural analysis. Hence, we heated the sample up to 1300 K at 43 GPa for few minutes. The first diffraction pattern collected, about 1 minute into the heating, showed new sharp peaks indicating that extensive recrystallization readily occurred. About 1000 peaks were indexed with few grains of a single orthorhombic phase. The *a* and *b* lattice parameters are similar to those of the *oS*8 phase, while the *c* parameter is roughly 3 times longer than the corresponding length in *oS*8 (Table 1). Inspection of structure factors indicates *Cmcm* as the most plausible space group. Structural solution and refinements were performed using the integrated intensities of the largest crystals identified in two multigrain patterns collected from different sample locations [31]. We found that at ~ 43 GPa and 1300 K GaP crystallizes with the structure type first observed in InSb at ~ 5 GPa [1], hereafter indicated with its Pearson notation *oS*24.

While the *oS*24 structure is described as a superstructure of *oS*8 [32], in GaP the two phases are substantially different. The relative translation and puckering of the NaCl-like layers results in the differentiation of the P atoms in *oS*24, with 2/3 of the P atoms (P1, point symmetry 8*f*) approaching and forming P-P bonds (Fig. 1a). Stacked perpendicularly to the *c*-axis a double layer with the out-of-plane P1-P1 bonds and the distorted in-plane P1-Ga squares alternates with a distorted NaCl-like layer containing the P2 atoms (point symmetry *4c*). Gallium is also in two non-equivalent crystallographic sites with different point symmetry and multiplicity (Table 1). All sites are fully occupied within uncertainty (~5%), showing that the phase is largely stoichiometric and ordered. Furthermore, all observed peaks are accounted for, ruling out the occurrence of significant chemical reactions during heating. The P1-P1 interatomic distance, around 2.2 Å, is by far, the shortest in the structure and is comparable to values observed in several compounds [33]. P1 is also coordinated by two Ga atoms at short distances; two at intermediate and two at long distances, resulting in a highly distorted coordination geometry. P2 does not form P-P bonds, it shows five short P-Ga bonds, while a sixth Ga atom lies at a markedly greater distance (Fig. 2b). Ga-P first coordination distances are spread in three groups (Fig. 2b): shorter lengths between 2.3 and 2.4 Å (close to the ambient conditions bond length, 2.358 Å), intermediate values around 2.5 Å, and distances that might reflect weak interactions, around 2.6 Å. The Ga-Ga shortest distances measure about 2.6 Å, which compares well with first coordination Ga-Ga distances found in elemental gallium at ambient conditions, suggesting that Ga-Ga weak interactions cannot be ruled out.

GaP-*oS*24 was compressed at ambient temperature up to ~ 50 GPa and then

decompressed to 18.6 GPa. The volume difference of *cF*8 and *oS*24 is ~18% at 25 GPa. Diffuse scattering lines connecting rows of Bragg's peaks along the *c*-axis direction (Fig. 3) appeared in decompression. These effects were subtle when first detected, at 26.4 GPa, but quickly gain intensity, demonstrating a rapid loss of long range ordering in the *c*-axis direction. It appears that while the NaCl-like layers are preserved, they experience a relative displacement, which might be driven by the breakdown of the dimers. Hence the onset of instability of *oS*24 in decompression can be placed between 30 and 26.4 GPa implying that there is no metastable coexistence at ambient temperature of *cF*8 and *oS*24.

The relative stability of four GaP polymorphs (i.e., oS24, cF8, CP16, and oS8) was investigated in this study using DFT. The total energy and enthalpy of the three phases characterized in our experiments and of *cP*16, a phase previously found stable in the pressure range here investigated [34,35], are compared as shown in Fig. 4. A good agreement between predicted and observed compressibility was obtained for all phases. Furthermore, because calculations typically overestimate volumes, we believe that the experimental volumes of *oS*8 obtained in this study are more realistic than literature values. Fig. 4(a) shows the calculated binding energy curves, suggesting several possible pressure-induced structural transitions. Calculations predict the low-pressure *cF*8 phase undergoes a phase transition to a high-pressure phase adopting the *cP*16 structure, followed by the orthorhombic phase o*S*24 at greater pressure. The calculated narrow stability range of *cP*16 is similar to what was found in earlier theoretical results [16] and to the behavior theoretically predicted and experimentally confirmed for the more thoroughly studied GaAs. While considering *oS*8 as a possible high-pressure phase of GaP above 20 GPa, we propose a different type of *Cmcm* in a 24-atom basis (*oS*24) from the current high-pressure XRD measurement of GaP. As shown in Fig. 4a), while *oS*24 has the lowest total energy at all pressures above 18 GPa, *oS*8 and *oS*24 are almost energetically degenerate. Conversely, the comparison of enthalpies (Fig. 4b) clearly shows that *oS*8 is never energetically favored in the pressure range explored in our analysis. We also considered site disordered states in *oS*8 and found them to have higher energy than the ordered states by 0.79 and 0.68 eV when a site-disorder was created in the unit cell containing 8 atoms at 20 and 29.3 GPa, respectively, in our calculations. The onset of the *oS*24 instability upon decompression was observed to occur at a pressure at which it is stable according to our calculations. It is plausible that the calculations underestimated the transition pressure, nonetheless, the stability of *cP*16 between *cF*8 and *oS*24 might explain the lack of metastable coexistence of the *cF*8 and *oS*24 phases. Further experiments at moderate temperature and fine pressure steps are required to assess the stability ranges of *cP*16 and *oS*24. We also calculated the physical properties of GaP (Table 2); we found that the band gap is closed in the orthorhombic phases, which

are both consistent with resistivity measurements.

Since our energetic analysis shows that above 18 GPa the *oS*24 phase is thermodynamically stable relative to *cF*8, *cP*16 and *oS*8, the latter phase, obtained in compression without heating, is metastable. In alternative, considering the high strain observed in *oS*8, the similarities of the *oS*8 and *oS*24 lattices and of their diffraction patterns, it is plausible that the "disordered *oS*8" might actually be a phase with a very high defect concentration in which *oS*24-like clusters might form locally[1]. Such scenario could explain the discrepancy between the ordering range obtained in diffraction and XAFS analysis [13]. While in InSb *oS*24 and *oS*8 were shown to be nearly equivalent arrangements, as they provide the same local configuration (i.e. number of like and unlike neighbor atoms) [32], in GaP the two phases differ markedly. The oS24 phase is more energetically favorable than oS8, for example, by 0.05 eV at 20 GPa and 0.08 eV at 40 GPa. The superstructure allows for the development of a strong bonding anisotropy, more apparent here compared to InSb [1,32] and in InAs [36]. GaP-*oS*24 shows short P-P dimers, a spread of Ga-P bond lengths and distorted coordination geometries. While the site-disordered *oS*8 implies nearly degenerate like and unlike atoms bonding, in *oS*24 we observe a strong directional covalent bond that explains the symmetry lowering and structural anisotropy of the phase. In GaP we finally understand the nature of the structural complexity of semiconductors at high pressure, a puzzling finding as it was assumed that the bonding character changes uniformly loosing directionality with pressure. Dimerization has not been considered to play an important role in the systematic of semiconductors polymorphism, even though the shortest interatomic distances occur between like atoms also in InSb-*oS*24 [1] and InAs [36]. Only recently in BP [37], phosphorous was shown to form chains in a superconducting phase at ~ 1 Mbar. Our results demonstrate that the concepts so far used to rationalize the systematics of semiconductors polymorphism such as the degree of ionicity, ionic sizes, electronegativity and the instability of structures with like atoms proximity cannot always describe the nature of polymorphism of binary semiconductors.

This research was sponsored by the National Nuclear Security Administration under the Stewardship Science Academic Alliances program through DOE Cooperative Agreement No. DE-NA0001982. This work performed under the auspices of the U.S. Department of Energy by Lawrence Livermore National Laboratory under Contract DE-AC52-07NA27344. EK acknowledges funding supported by the National Aeronautics and Space Administration under

[1] Because our powder patterns suffer of preferred orientation, we cannot argue which structural model is most likely correct. Calculated diffraction pattern of oS24 do not show strong peaks at low angle, which led to suggest site disordering of oS8.

Agreement No. NNX10AN23H issued through the NASA Space Grant. Sandia National Laboratories is a multiprogram laboratory operated by Sandia Corporation, a wholly owned subsidiary of Lockheed Martin Company, for the United States Department of Energy's National Nuclear Security Administration under Contract DE-AC04-94AL85000. This work was conducted at HPCAT (Sector 16), Advanced Photon Source (APS), Argonne National Laboratory. HPCAT operations are supported by DOE- NNSA under Award No. DE-NA0001974 and DOE-BES under Award No. DE-FG02-99ER45775, with partial instrumentation funding by NSF. APS is supported by DOE-BES, under Contract No. DE-AC02-06CH11357. We thank Sergey Tkachev for his assistance with the gas loadings. Use of the COMPRES-GSECARS gas loading system was supported by COMPRES under NSF Cooperative Agreement EAR 11-57758 and by GSECARS through NSF grant EAR-1128799 and DOE grant DE-FG02-94ER14466. The sample was kindly made available for this study by Prof. Malcolm Nicol.

Figure 1. Experimental and calculated P-V data of GaP polymorphs. Solid black squares: *cF*8 SXD; open black squares: *cF*8 pXRD; black broken line: *cF*8 experimental EOS; blue circles: *oS*8 pXRD; blue diamonds: *oS8* literature [12,13]; red solid squares: *oS24*; red crosses: *oS24* showing weak diffuse scattering lines; black, green, blue and red solid lines with triangles: calculated volumes per formula unit of *cF*8, *cP*16, *oS*8 and *oS*24 respectively.

Figure 2. A) The structure of *oS*24 is represented [38] with blue P1 atoms forming P-P bonds between layers and purple P2 atoms bonded to the green Ga atoms. B) Interatomic distances in GaP-*oS*24. Blue crosses: P1-P1; orange symbols: P1-Ga; purple symbols: P2-Ga; black triangles: Ga-Ga. Solid symbols represent distances with multiplicity 2.

Figure 3. Details of diffraction patterns of GaP-*oS*24. Diffuse scattering lines between Bragg's peaks are developed in decompression.

Figure 4. The calculated energetics of GaP: (a) Total energy vs. volume and (b) enthalpy vs. volume.

Table 1. Structural parameters of GaP-*oS*24.

	Experimental	Calculated
P (GPa)	42.7	42
T (K)	298	0
a (Å)	4.621 (2)	4.679
b (Å)	4.927 (2)	4.981
c (Å)	13.335(7)	13.275
V (Å^3)	303.27	309.39

Atomic fractional coordinates		
P1 (8*f*)	0, 0.3890(8), 0.0703(6)	0, 0.38982, 0.07177
P2 (4*c*)	0, 0.1084(12), 1/4	0, 0.11056, 1/4
Ga1 (8*f*)	0, 0.1064(4), 0.5909(2)	0, 0.10788, 0.59030
Ga2 (4*c*)	0, 0.5849(5), 1/4	0, 0.58698, 1/4

The experimental unit cell parameters were determined from least squares refinement against the *d*-spacing of 345 peaks. The refinement of atomic parameters was performed against squared structure factors (N_{all} =115, R_{eq} =12%, R_σ =7.5%). The refinement converged with satisfactory statistical parameters (R_1=6.5%, $R_{4\sigma}$=6.7%, wR_2=17.5%).

Table 2. The calculated physical properties of GaP. The number in parenthesis is from reference [39].

Pressure (GPa)	0	16.5	24	24
Crystal structure	*cF*8	*cP*16	*oS*8	*oS*24
Lattice constants (Å)	5.525	6.07	4.782 4.975 4.603	4.805 5.092 13.803
E_g (eV)	1.65 (2.26)	0.35	0.0	0.0

References

[1] R. J. Nelmes and M. I. McMahon, Phys. Rev. Lett. **74**, 106 (1995).
[2] S. Minomura and H. G. Drickamer, J. Phys. Chem. Solids **23**, 451 (1962).
[3] C. G. Homan, D. P. Kendall, T. E. Davidson, and J. Frankel, Solid State Commun. **17**, 831 (1975).
[4] M. I. McMahon and R. J. Nelmes, J. Phys. Chem. Solids **56**, 485 (1995).
[5] R. J. Nelmes, M. I. McMahon, N. G. Wright, D. R. Allan, H. Liu, and J. S. Loveday, J. Phys. Chem. Solids **56**, 539 (1995).
[6] M. I. McMahon and R. J. Nelmes, Phys. Status Solidi B **198**, 389 (1996).
[7] R. J. Nelmes and M. I. McMahon, Semicond. Semimet. **54**, 145 (1998).
[8] G. J. Ackland, Rep. Prog. Phys. **64**, 483 (2001).
[9] A. Mujica, A. Rubio, A. Muñoz, and R. J. Needs, Rev. Mod. Phys. **75**, 863 (2003).

[10] A. Zunger, K. Kim, and V. Ozolins, Phys. Status Solidi B **223**, 369 (2001).
[11] M. B. Jr and A. L. Ruoff, J. Appl. Phys. **53**, 6179 (1982).
[12] R. J. Nelmes, M. I. McMahon, and S. A. Belmonte, Phys. Rev. Lett. **79**, 3668 (1997).
[13] G. Aquilanti, H. Libotte, W. A. Crichton, S. Pascarelli, A. Trapananti, and J.-P. Itié, Phys. Rev. B **76**, 64103 (2007).
[14] O. Arbouche, B. Belgoumène, B. Soudini, Y. Azzaz, H. Bendaoud, and K. Amara, Comput. Mater. Sci. **47**, 685 (2010).
[15] L. Li, W. Jian-Jun, A. Xin-You, W. Xue-Min, L. Hui-Na, and W. Wei-Dong, Chin. Phys. B **20**, 106201 (2011).
[16] A. Mujica and R. J. Needs, Phys. Rev. B **55**, 9659 (1997).
[17] H. Cynn, B. J. Baer, S. G. MacLeod, W. J. Evans, M. J. Lipp, J. P. Klepeis, Z. Jenei, J. Y. Chen, K. Catalli, D. Popov, and C. Y. Park, in (2012).
[18] C. W. Greeff, J. C. Boettger, M. J. Graf, and J. D. Johnson, J. Phys. Chem. Solids **67**, 2033 (2006).
[19] V. B. P. Mark Rivers, High Press. Res. **28**, 273 (2008).
[20] Y. Fei, A. Ricolleau, M. Frank, K. Mibe, G. Shen, and V. Prakapenka, Proc. Natl. Acad. Sci. **104**, 9182 (2007).
[21] Y. Meng, R. Hrubiak, E. Rod, R. Boehler, and G. Shen, Rev. Sci. Instrum. **86**, 72201 (2015).
[22] A. P. Hammersley, S. O. Svensson, M. Hanfland, A. N. Fitch, and D. Hausermann, High Press. Res. **14**, 235 (1996).
[23] P. Dera, K. Zhuravlev, V. Prakapenka, M. L. Rivers, G. J. Finkelstein, O. Grubor-Urosevic, O. Tschauner, S. M. Clark, and R. T. Downs, High Press. Res. **33**, 466 (2013).
[24] G. M. Sheldrick, Acta Crystallogr. A **64**, 112 (2008).
[25] G. Kresse and J. Furthmüller, Phys. Rev. B **54**, 11169 (1996).
[26] J. P. Perdew and Y. Wang, Phys. Rev. B **45**, 13244 (1992).
[27] P. E. Blöchl, Phys. Rev. B **50**, 17953 (1994).
[28] G. Kresse and D. Joubert, Phys. Rev. B **59**, 1758 (1999).
[29] M. Methfessel and A. T. Paxton, Phys. Rev. B **40**, 3616 (1989).
[30] H. J. Monkhorst and J. D. Pack, Phys. Rev. B **13**, 5188 (1976).
[31] B. Lavina, P. Dera, and Y. Meng, J Vis Exp e50613 (2013).
[32] A. A. Kelsey and G. J. Ackland, J. Phys. Condens. Matter **12**, 7161 (2000).
[33] A. H. Cowley, Chem. Rev. **65**, 617 (1965).
[34] J. Crain, R. O. Piltz, G. J. Ackland, S. J. Clark, M. C. Payne, V. Milman, J. S. Lin, P. D. Hatton, and Y. H. Nam, Phys. Rev. B **50**, 8389 (1994).
[35] A. Mujica, R. J. Needs, and A. Muñoz, Phys. Rev. B **52**, 8881 (1995).
[36] J. López-Solano, A. Muñoz, and A. Mujica, Phys. Status Solidi B **244**, 274 (2007).
[37] X. Zhang, J. Qin, H. Liu, S. Zhang, M. Ma, W. Luo, R. Liu, and R. Ahuja, Sci. Rep. **5**, 8761 (2015).
[38] K. Momma and F. Izumi, J. Appl. Crystallogr. **44**, 1272 (2011).
[39] B. G. Streetman, *Solid State Electronic Devices* (Prentice Hall New Jersey, n.d.).

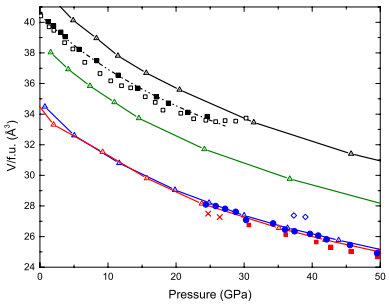

Fig. 1

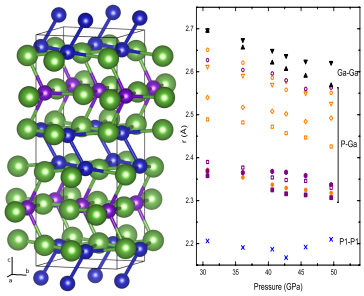

Fig. 2

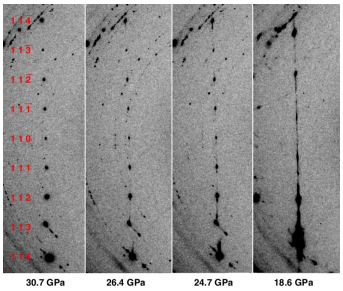

Fig. 3

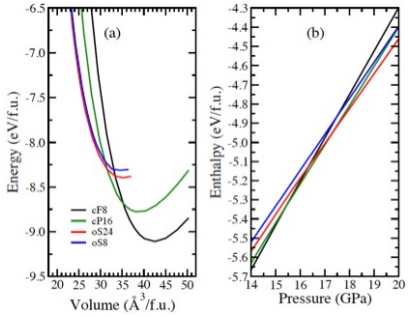

Fig. 4